Acta Astronautica 178 (2021) 743–756

Contents lists available at ScienceDirect

Acta Astronautica

journal homepage: www.elsevier.com/locate/actaastro

Observational properties of low-energy orbits around icy moons

Francisco Salazar [a], Elena Fantino [a,*], Elisa Maria Alessi [b,c]

[a] Department of Aerospace Engineering, Khalifa University of Science and Technology, P.O. Box 127788, Abu Dhabi, United Arab Emirates

[b] Istituto di Matematica Applicata e Tecnologie Informatiche "Enrico Magenes", Consiglio Nazionale delle Ricerche, Via Alfonso Corti 12, 20133 Milano, Italy

[c] Istituto di Fisica Applicata "Nello Carrara", Consiglio Nazionale delle Ricerche, Via Madonna del Piano 10, 50019 Sesto Fiorentino (FI), Italy

ARTICLE INFO

MSC:
70F15
70F07

Keywords:
Circular restricted three-body problem
Planar Lyapunov orbits
Homoclinic connections
Heteroclinic connections
Icy moons

ABSTRACT

The moons of the giant planets are getting into the focus of the next exploration missions to the outer solar system. The reason for this interest resides in their dynamical role within their respective systems and the signs of habitability suggested in some cases by surface and subsurface features. Flyby missions offer adequate recognition scenarios for the initial exploration phase of a celestial body, but they must be followed by orbiters if more extended observations are required. The dynamical structures of the Circular Restricted Three-Body Problem pave the way to such opportunities. In particular, libration point orbits around the two collinear equilibrium points L_1 and L_2 of a planet–moon-spacecraft system are characterized by low speeds relative to the moon. Heteroclinic and homoclinic connections built from these orbits allow close-up views of the moons. The aim of this work is to determine the observational performance of heteroclinic and homoclinic connections of planar Lyapunov orbits around L_1 and L_2 for three systems of scientific relevance: Jupiter–Europa, Uranus–Titania and Uranus–Oberon. Lunar surface coverage, repeat patterns, lunar distance ranges and speed profiles are derived and discussed for each case.

1. Introduction

The aim of this work is to propose a new approach to observe planetary moons in the solar system. The main challenge in this framework is given by the perturbing effect of the gravity of the planet. Although low-altitude, near-polar orbits that could cover the entire surface of the satellite are dynamically unstable [1,2], previous studies for planetary orbiters have managed to identify long-term stable orbits around the moons [3–6]. In particular, Paskowitz & Scheeres [3,4] studied temporarily captured trajectories in Hill's problem (the limit case of the Circular Restricted Three-Body Problem, CR3BP, in which the mass ratio of the system tends to zero, see also [7] pp. 602–629) with application to orbits about Europa, and identified orbits that are stable over long time spans. They analyzed the doubly-averaged equations of motion for the orbital elements of the spacecraft at the moon, looking for stable equilibrium solutions. By applying a global grid search in the Jupiter–Europa CR3BP, Russell [5] identified a family of three-dimensional periodic orbits at Europa. Similarly, Russell & Lara [6] found long-term stable orbits in the Saturn–Enceladus unaveraged perturbed Hill's model by performing a global grid search. Stable solutions about Enceladus were identified at altitudes near 200 km and inclinations approaching 65°.

In this study, the effect of the planet's gravity is included by adopting the CR3BP. The existence of periodic solutions around the collinear libration points L_1 and L_2 in the CR3BP and the characteristics of their stable and stable hyperbolic invariant manifolds (HIMs) allow to design trajectories that connect the two libration point regions and coast around the moon at low relative speed. The objective of this work is to design homoclinic trajectories, i.e., transfers departing and reaching the same periodic orbit around L_1 or L_2, and heteroclinic connections between periodic orbits at L_1 and L_2 [8–10] and assess their performance as science orbits in the context of a lunar exploration mission. Thanks to the periodic character of the departure and arrival libration point orbits, several close approaches to the moon can be carried out, and the periodic orbits can be used to park the spacecraft between consecutive transfers. Furthermore, homoclinic and heteroclinic trajectories requiring negligible amounts of propellant exist. Given the distances of these systems from the Earth, missions of this type can only be operated with autonomous onboard navigation. For the most recent developments in this area, the reader is referred to [11].

In the past, heteroclinic connections have been used in the Sun–Earth [12] and Earth–Moon systems [13] and proposed in the Jovian [8,14], Saturnian [15,16] and Uranian systems [17]. In Jupiter's system, the Petit Grand Tour [14,18] described the possibility of using low-energy transfers of all kinds to tour the moons, while Alessi & Pergola [19] explored a temporary capture based on HIMs to observe

* Corresponding author.
E-mail addresses: e7940@hotmail.com (F. Salazar), elena.fantino@ku.ac.ae (E. Fantino), elisamaria.alessi@cnr.it (E.M. Alessi).

https://doi.org/10.1016/j.actaastro.2020.09.051
Received 9 January 2020; Received in revised form 30 June 2020; Accepted 30 September 2020
Available online 3 October 2020
0094-5765/

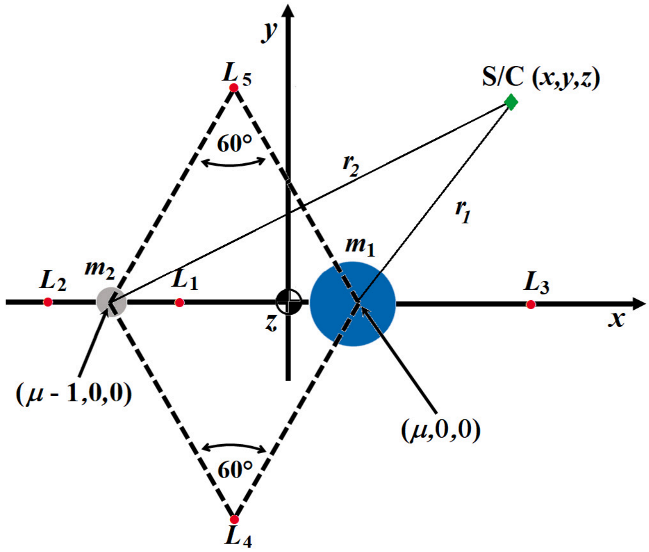

Fig. 1. Representation of the CR3BP of primaries m_1 and m_2 in the synodical barycentric reference frame.

Callisto. Nonetheless, to the best of the authors' knowledge, a systematic study on the benefits of low-energy orbits for observational purposes is missing.

In this work, the systems of Jupiter and Europa, Uranus and Titania and Uranus and Oberon are modeled as planar CR3BPs. These moons are chosen because the future generation of exploration missions in the outer solar system focuses on the observation of the planetary systems of, in particular, Jupiter and Uranus [20]. These planets host icy moons for which scientists have predicted the existence of subsurface oceans [21–25]. The evidence for water vapor plumes near Europa's south pole supports this hypothesis, thereby calling for a scientific search for potential habitability [22–25]. Then, since Titania and Oberon are the most massive moons in Uranus' system and their composition includes rock and water ice in equal proportions, they are suitable targets in the search for underground oceans [26].

Jupiter's system is the scene of two fundamental missions – ESA's JUICE and NASA's Europa Clipper – that will be launched in 2022 and 2025, respectively. JUICE will study Jupiter and its icy moons, focusing on the characterization of Ganymede, Callisto and Europa, and evaluating their potential to support life [27]. Similarly, Europa Clipper will explore Europa to confirm the existence of water within its icy surface and investigate its habitability [28]. A number of missions to Uranus have been proposed, e.g., Uranus Pathfinder [26,29], ODINUS [30] and OCEANUS [31]. If an orbit insertion at a given moon is not feasible due to the propellant budget, the usual approach is to collect observational data by means of consecutive flybys.

In this work, the kinematical and observational features of heteroclinic and homoclinic connections between the collinear points L_1 and L_2 of CR3BPs with a giant planet and one of its moons as primaries are analyzed and some preliminary conclusions on their possible scientific exploitation are drawn. The performance of these low-energy trajectories as observation orbits around planetary moons is assessed by evaluating speeds, altitudes, times of flight and lunar surface coverage. The planar approximation of the CR3BP is assumed because the inclinations of the orbital planes of Europa, Titania and Oberon with respect to Jupiter's and Uranus' equators, respectively, are smaller than one degree and the orbital eccentricities of these moons are negligible [32]. Hence, their orbits are approximately circular and contained in the planet's equatorial plane. The planar Lyapunov orbits (PLOs) around L_1 and L_2 and their heteroclinic and homoclinic connections are 2D orbits. Therefore, using these trajectories, the spacecraft can make simultaneous observations of the northern and southern hemisphere of a moon in search for extended features, such as the mentioned subsurface oceans. Three-dimensional solutions (obtained, for example, with the aid of halo orbits) would allow to explore the polar regions but at the cost of a change-of-plane maneuver. This option has been studied in a research specifically devoted to Enceladus [33]. The planar approximation presented here is aligned with previous investigations [16,34,35], in which spacecraft cyclers of the Galilean moons and the Inner Large Moons of Saturn are designed in 2D, using PLOs and impulsive maneuvers or low-thrust propelled arcs.

The paper is organized as follows. Section 2 illustrates the dynamical model, describes the families of PLOs around L_1 and L_2 used in this work and illustrates the procedure employed to design homoclinic and heteroclinic connections. Section 3 presents the solutions and discusses their observational properties. The conclusions are drawn in Section 4.

2. The dynamical model, the periodic orbits and their connections

2.1. The CR3BP

The CR3BP [7] models the motion of a massless body subject to the gravitational attraction of two primaries of mass m_1 (planet) and m_2 (moon) in circular orbits around their common center of mass, whereas the third body (the spacecraft) has negligible mass. The dynamical system is characterized by one parameter, i.e., the mass ratio $\mu = m_2/\left(m_1 + m_2\right)$. The equations of motion are referred to the synodical barycentric reference frame, where m_1 and the m_2 occupy the fixed positions $(\mu, 0, 0)$ and $(\mu - 1, 0, 0)$ on the x-axis, as illustrated in Fig. 1. In dimensionless variables, using μ and d as reference magnitudes, the mean motion of the primaries has unit value, whereas their orbital period T equals 2π.

The motion of the spacecraft in the synodical barycentric reference frame is governed by the following system of equations:

$$\begin{aligned} \ddot{x} - 2\dot{y} &= \frac{\partial \Omega}{\partial x}, \\ \ddot{y} + 2\dot{x} &= \frac{\partial \Omega}{\partial y}, \\ \ddot{z} &= \frac{\partial \Omega}{\partial z}, \end{aligned} \tag{1}$$

where

$$\Omega(x, y, z) = \frac{x^2 + y^2 + z^2}{2} + \frac{1-\mu}{r_1} + \frac{\mu}{r_2} + \frac{\mu(1-\mu)}{2}, \tag{2}$$

x, y and z are the position coordinates of the spacecraft and r_1 and r_2 are its distances from the two primaries, as shown in Fig. 1.

The CR3BP admits one integral of motion, the Jacobi constant C_J, related to the mechanical energy E of the third body by the expression

$$C_J = -\left(\dot{x}^2 + \dot{y}^2 + \dot{z}^2\right) + 2\Omega\left(x, y, z\right) = -2E. \tag{3}$$

Five equilibrium points denoted L_i, $i = 1, \ldots, 5$, further characterize the system. The first three, the so-called collinear points, lie on the x-axis at positions which depend on the value of μ. L_4 and L_5 form equilateral triangles with the primaries. Table 1 reports the basic parameters of the CR3BPs of Jupiter–Europa, Uranus–Titania and Uranus–Oberon considered in this work.

2.2. The periodic orbits

The linear approximation of the dynamics in the neighborhood of a given equilibrium point leads to families of libration point orbits (LPOs) [7]. As mentioned before, the PLOs about L_1 and L_2 are considered because their periodic character makes them convenient parking orbits in the framework of a complex multi-body observation tour [16,

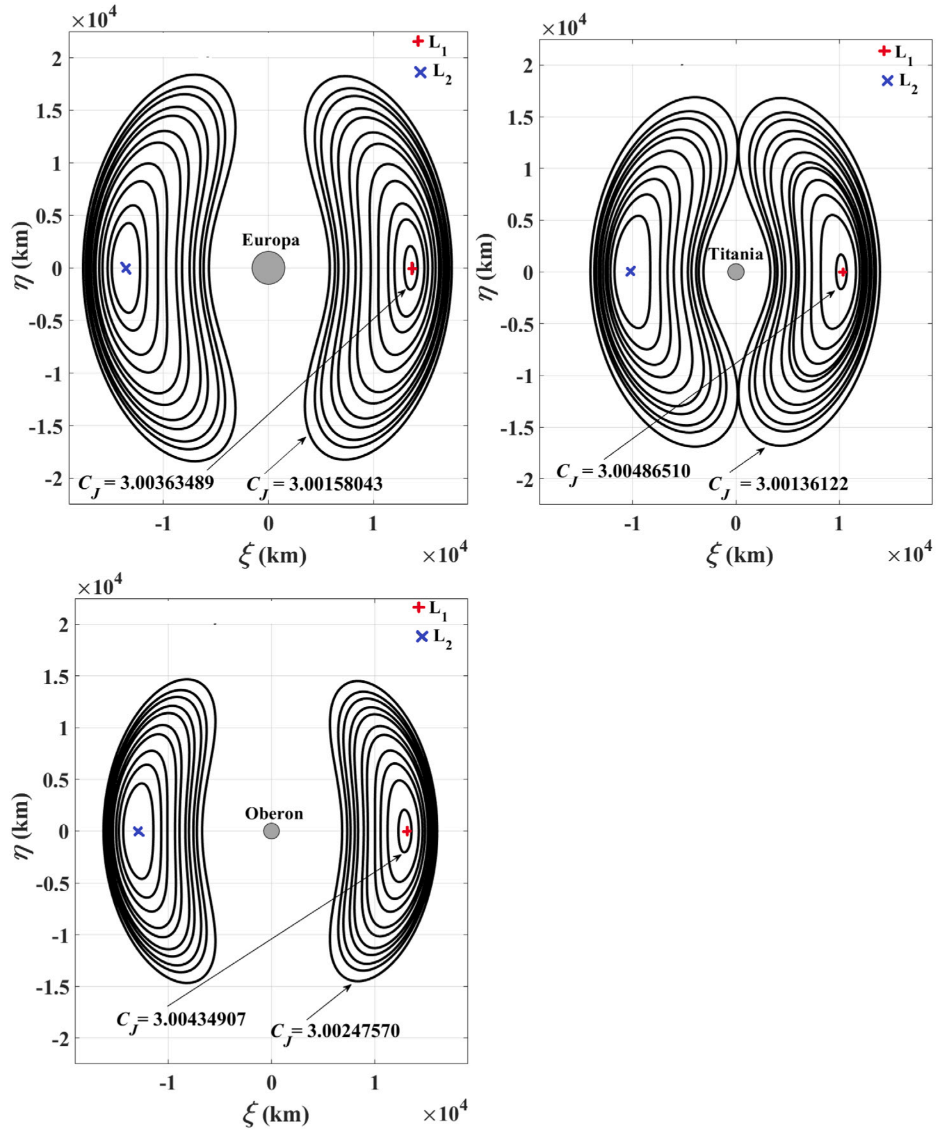

Fig. 2. PLOs around L_1 and L_2 in the three systems for the range of Jacobi constant values indicated in Table 2. The reference frame is synodical and centered at the moon.

Table 1
Mass ratio μ, distance d between primaries, orbital period T and physical radius R of the moon for the CR3BPs considered [32].

CR3BP	μ $(\cdot 10^{-4})$	d $(\cdot 10^5$ km)	T (day)	R (km)
Jupiter–Europa	0.25285825	6.7110	3.60	1560.8
Uranus–Titania	0.39393160	4.3591	8.70	788.9
Uranus–Oberon	0.33213369	5.8352	13.46	761.4

Table 2
Minimum and maximum values of C_J of the PLOs around L_1 and L_2 for the CR3BPs studied in this work.

CR3BP	min C_J	max C_J
Jupiter–Europa	3.00158043	3.00363489
Uranus–Titania	3.00136122	3.00486510
Uranus–Oberon	3.00247570	3.00434907

17,34,36], while allowing to approach the moon in its equatorial plane. From there, large portions of the northern and southern hemisphere are visible. Table 2 reports the selected limits of the intervals of C_J of the PLOs in the three systems. Fig. 2 shows the families of PLOs around L_1 and L_2 in the three systems for the ranges of Jacobi constant values indicated in Table 2. In this figure, the greek letters ξ and η denote the axes of a synodical reference frame centered at the moon. The coordinates are rescaled to km via multiplication by d. The lower limit of the C_J range corresponds to the largest orbit in the family. This limit satisfies a requirement on the y-amplitude set by the concept design of the lunar cycler described in Refs. [16,34,35], in which the PLOs of the families are used to move between moons using a planet-spacecraft two-body approximation. The PLOs must be contained in the region of influence of the moon and this limits their size and, therefore, the minimum value of the Jacobi constant in the family. The maximum

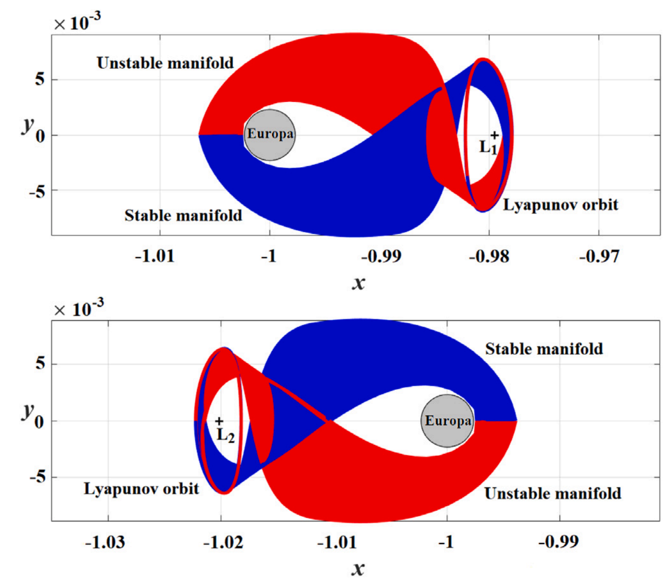

Fig. 3. Branches of the stable and unstable HIMs associated with PLOs with C_J = 3.00350250 around L_1 (top) and L_2 (bottom) in Jupiter–Europa's CR3BP. Synodical barycentric reference frame and dimensionless coordinates.

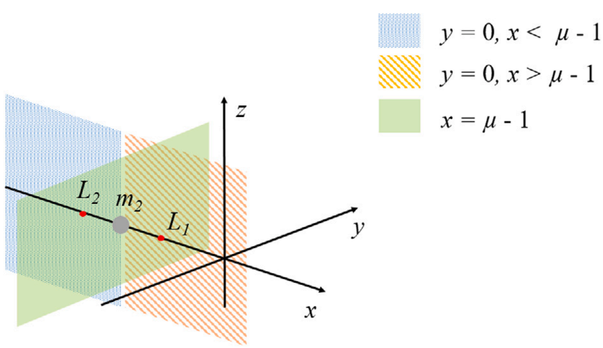

Fig. 4. The planar sections employed to calculate the three types of transfers.

value of C_J corresponds to the smallest orbit in the family. As shown below, this upper limit includes all the useful orbits at the high end of the C_J spectrum.

2.3. Homoclinic and heteroclinic connections

It is known that the initial states of the stable/unstable HIMs of PLOs can be linearly approximated by applying a suitable small perturbation in the direction of the stable/unstable eigenvector associated with the monodromy matrix, after an appropriate time transformation through the state transition matrix [37]. Positive and negative branches can then be computed by numerical propagation. The stable manifold approaches the periodic orbit forward in time; the unstable manifold does it backward in time. As an example, Fig. 3 shows individual branches of the stable and unstable manifolds of the PLO around L_1 (top) and L_2 (bottom) with C_J = 3.00350250 in the Jupiter–Europa synodical barycentric reference frame.

Heteroclinic and homoclinic connections are here computed by propagating suitable branches of the HIMs of PLOs till their first

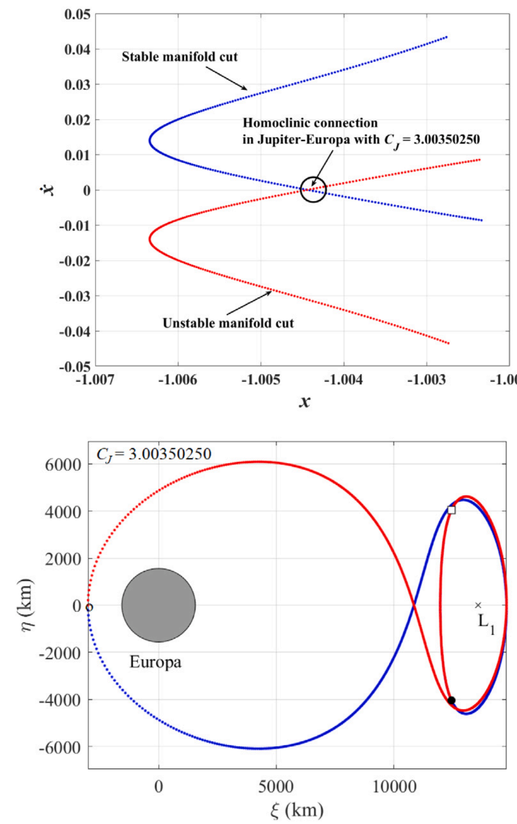

Fig. 5. Construction of a homoclinic loop from a PLO around L_1 with C_J= 3.00350250 in the Jupiter–Europa CR3BP. Top: Intersections of the stable and unstable HIMs with $\Sigma : \{y = 0, x < \mu - 1\}$. Bottom: the homoclinic connection in configuration space.

crossing with a suitable Poincaré section Σ. Three planar sections have been used to compute the connections (see Fig. 4):

- $\Sigma : \{y = 0, x < \mu - 1\}$ for homoclinic connections of PLOs around L_1;
- $\Sigma : \{y = 0, x > \mu - 1\}$ for homoclinic connections of PLOs around L_2;
- $\Sigma : \{x = \mu - 1, \dot{x} > 0\}$ for heteroclinic connections from PLOs around L_2 to PLOs around L_1 (due to symmetry, the equivalent connections from L_1 to L_2, which would correspond to the condition $\dot{x} < 0$ on Σ, are geometrically identical to these, hence they have not been computed).

The heteroclinic transfers designed in this work always occur between orbits with the same value of the Jacobi constant. The intersections of the HIMs with Σ are the phase-space cuts of the trajectories with a given Poincaré surface. These cuts are approximated by implementing a bisection scheme on the numerical propagation of the trajectories through Σ. The state vectors (position and velocity) obtained in this way are then projected on the $x\dot{x}$-plane (homoclinic case) or the $y\dot{y}$-plane (heteroclinic case) where they form curves. The states corresponding to the points of intersections (if any) between

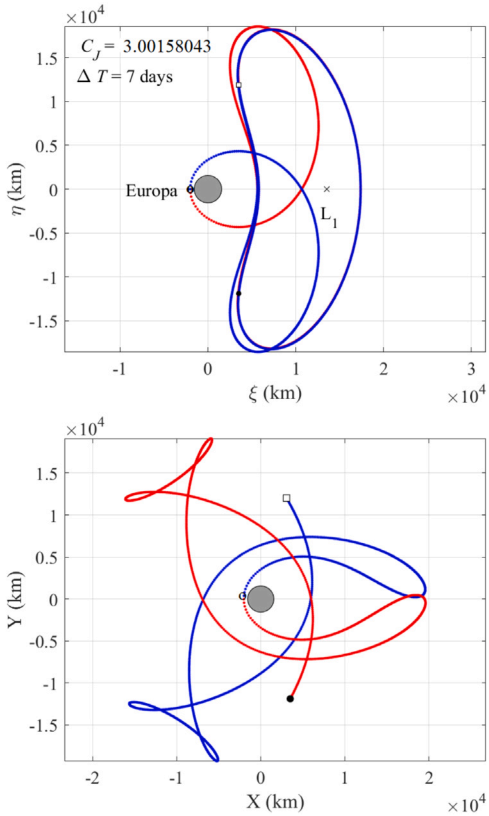

Fig. 6. Homoclinic connection in the Jupiter–Europa system from/to a PLO around L_1 with $C_J = C_J^*$. Top: synodic moon-centered frame. Bottom: inertial moon-centered frame.

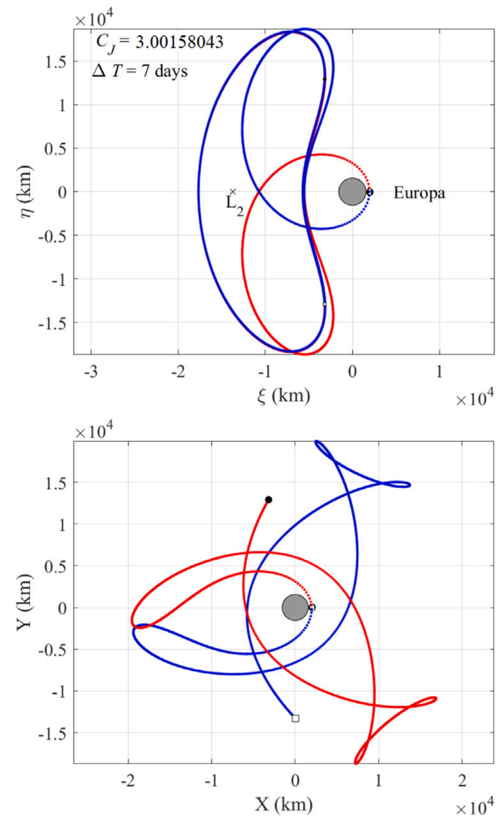

Fig. 7. Homoclinic connection in the Jupiter–Europa system from/to a PLO around L_2 with $C_J = C_J^*$. Top: synodic moon-centered frame. Bottom: inertial moon-centered frame.

curves enable the connections between PLOs. The errors in position and velocity introduced by the approximations are 1 km and 0.1 m/s, respectively, and can be made smaller in a more refined analysis. Therefore, the transfer from the unstable to the stable manifold can be considered maneuver free. As an example, Fig. 5 (top) shows the cut of the stable and unstable HIMs of a PLO around L_1 in the Jupiter–Europa system with $\Sigma : \{y = 0, x < \mu - 1\}$. The intersection between the curves indicates the existence of a homoclinic connection (Fig. 5 bottom). The time of flight ΔT for this transfer is 5 days.

3. Results

For each system, the PLO families have been populated using a constant separation in C_J. The procedure starts by constructing a set of orbits around one of the two equilibrium points in the selected C_J range by a very fine continuation on the x-coordinate of the initial state (one of the intersections of the orbit with the x-axis). Then, the C_J range is divided into N intervals, and the orbits that most closely approximate the resulting discretization are retained. The family of the other libration point is populated from an equivalent initial fine set of orbits by choosing the members that best match the C_J values of the other family. In this work, $N = 25$.

Homoclinic and heteroclinic connections have been obtained for the three systems with the method described in the previous section. When two or more connections exist for the same transfer, i.e., if the curves resulting from the cut of the stable and unstable invariant manifold with Σ intersect in more than one point, the connection reaching closest to the moon has been chosen. Figs. 6 to 22 show a sample of homoclinic and heteroclinic connections for the Jupiter–Europa, Uranus–Titania, and Uranus–Oberon systems. Each transfer is displayed in the synodic moon-centered frame and in a frame centered at the

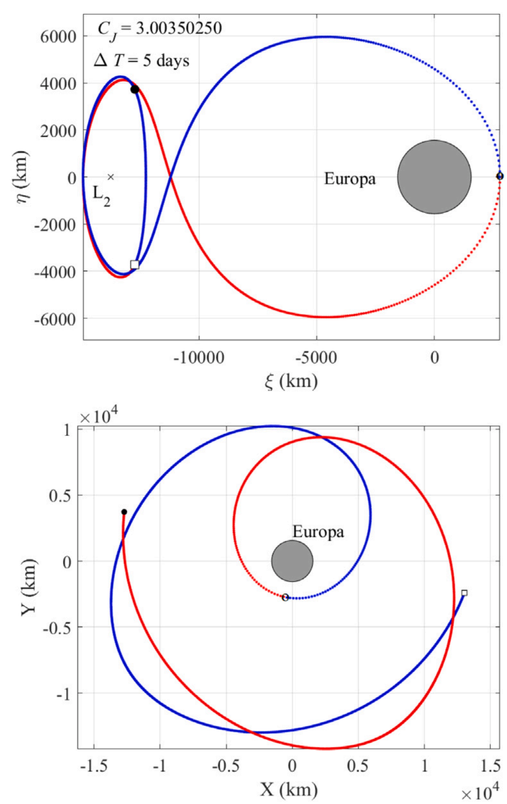

Fig. 8. Homoclinic connection in the Jupiter–Europa system from/to a PLO around L_2 with $C_J = C_J^{**}$. Top: synodic moon-centered frame. Bottom: inertial moon-centered frame.

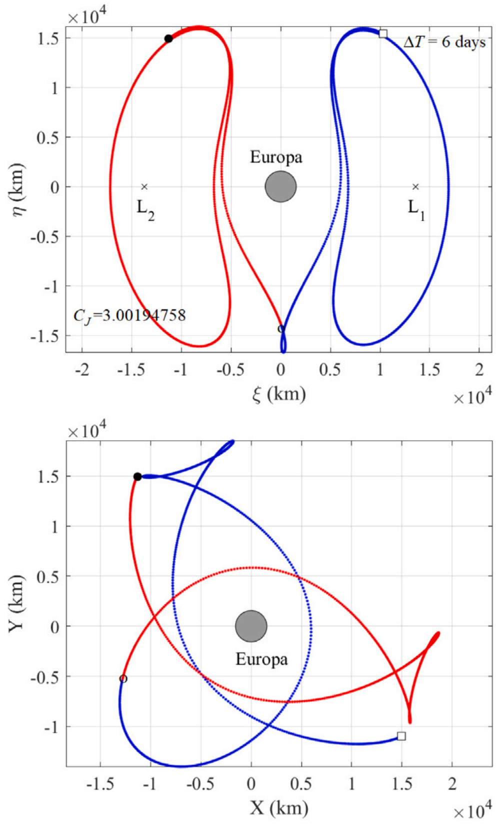

Fig. 9. Heteroclinic connection in the Jupiter–Europa system from a PLO around L_2 to a PLO around L_1 with $C_J = C_J^{*}$. Top: synodic moon-centered frame. Bottom: inertial moon-centered frame.

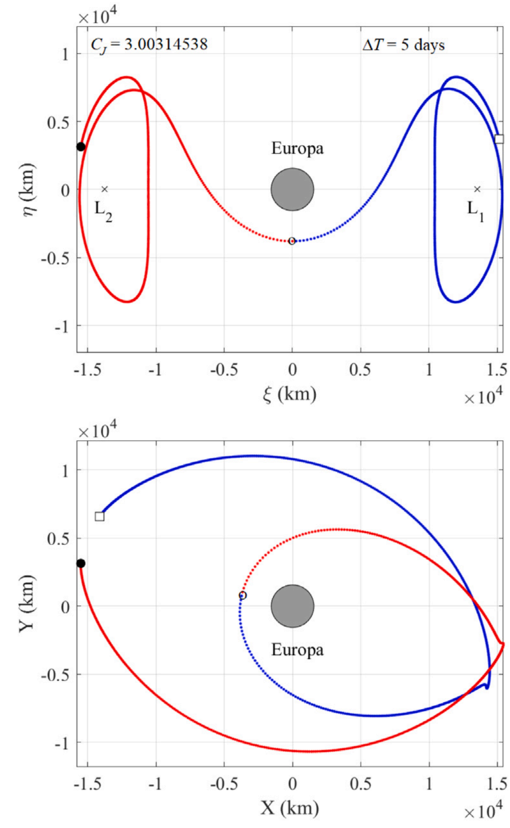

Fig. 10. Heteroclinic connection in the Jupiter–Europa system from a PLO around L_2 to a PLO around L_1 with $C_J = C_J^{**}$. Top: synodic moon-centered frame. Bottom: inertial moon-centered frame.

Table 3
Minimum (C_J^{*}) and maximum (C_J^{**}) values of the Jacobi constant for which homoclinic connections at L_1 and L_2 have been found in the three systems considered.

CR3BP	C_J^{*}	C_J^{**}
Jupiter–Europa	3.00158043	3.00350250
Uranus–Titania	3.00136121	3.00460450
Uranus–Oberon	3.00247569	3.00424496

Table 4
Minimum (C_J^{*}) and maximum (C_J^{**}) values of the Jacobi constant for which heteroclinic connections between L_2 and L_1 have been found in the three systems considered.

CR3BP	C_J^{*}	C_J^{**}
Jupiter–Europa	3.00194758	3.00314538
Uranus–Titania	3.00260864	3.00413865
Uranus–Oberon	3.00257934	3.00377664

moon with inertially-pointing axes, initially ($t = 0$) parallel to those of the synodic frame. The inertial frame representation gives an indication of the effect of the planetary gravity on the orbit of the spacecraft relative to the moon. The trajectories are sampled uniformly in time. Therefore, a lower density of points corresponds to a high-speed portion of the transfer, around the perilunes, whereas the apolunes are points of minimum for the velocity. The filled circle and the open square indicate the beginning and the end of a transfer, whereas the open circle refers to the matching point between the unstable and the stable trajectory arcs on Σ. The Jacobi constant C_J and the total transfer time ΔT are reported in the legend.

The minimum C_J^{*} and maximum C_J^{**} values of C_J for which transfers of each category (homoclinics and heteroclinics) have been found are reported in Tables 3 and 4, respectively.

3.1. Observational parameters

The geometrical and kinematical parameters of an orbit allow assessing its usefulness for observation purposes. Altitudes, speeds, flight times, instantaneous visible areas and durations of visibility windows are the primary factors in the design of a remote sensing mission. They are also drivers for instrument specifications, observing program definition and operations planning.

Table 5
Minimum (h_{min}) and maximum (h_{max}) altitudes above the lunar surface, minimum (v_{min}) and maximum (v_{max}) speeds with respect to a moon-centered inertial frame, times of flight ΔT through the homoclinic connections of PLOs around L_1 with Jacobi constant C_J in the three systems considered.

CR3BP	C_J	h_{min} (km)	h_{max} (km)	v_{min} (m/s)	v_{max} (m/s)	ΔT (day)
Jupiter–Europa	C_J^{*}	455	18 493	38	1653	7
Jupiter–Europa	C_J^{**}	1438	13 218	111	1275	5
Uranus–Titania	C_J^{*}	1421	18 808	23	452	23
Uranus–Titania	C_J^{**}	1910	10 469	25	351	12
Uranus–Oberon	C_J^{*}	237	16 533	5	595	24
Uranus–Oberon	C_J^{**}	1645	13 160	33	355	19

Tables 5 to 7 report the minimum (h_{min}) and maximum (h_{max}) altitudes above the lunar surface, the minimum (v_{min}) and maximum (v_{max}) speeds with respect to a moon-centered inertial frame (with axes inertially pointing and parallel to x and y at the beginning of a transfer, t=0) and the times of flight ΔT through the homoclinic and heteroclinic transfers shown in Figs. 6–22.

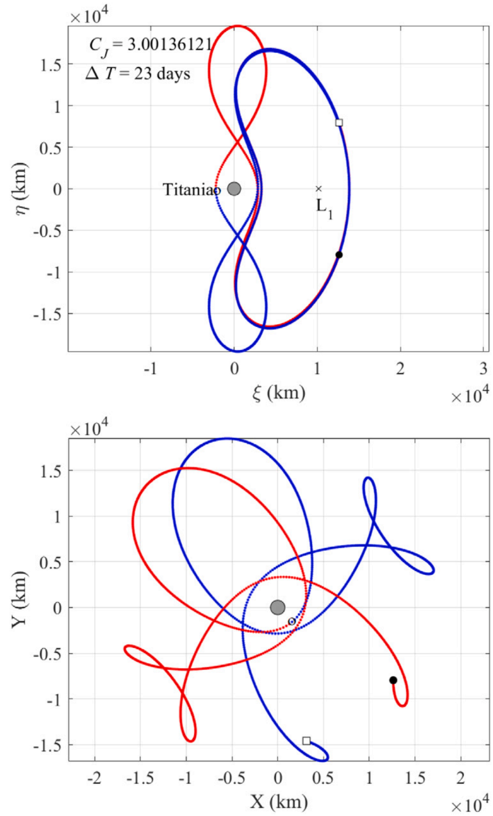

Fig. 11. Homoclinic connection in the Uranus–Titania system from/to a PLO around L_1 with $C_J = C_J^*$. Top: synodic moon-centered frame. Bottom: inertial moon-centered frame.

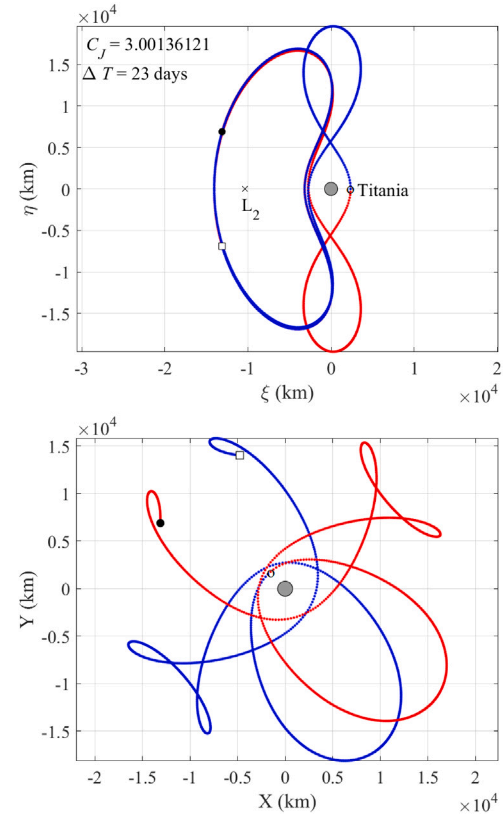

Fig. 13. Homoclinic connection in the Uranus–Titania system from/to a PLO around L_2 with $C_J = C_J^*$. Top: synodic moon-centered frame. Bottom: inertial moon-centered frame.

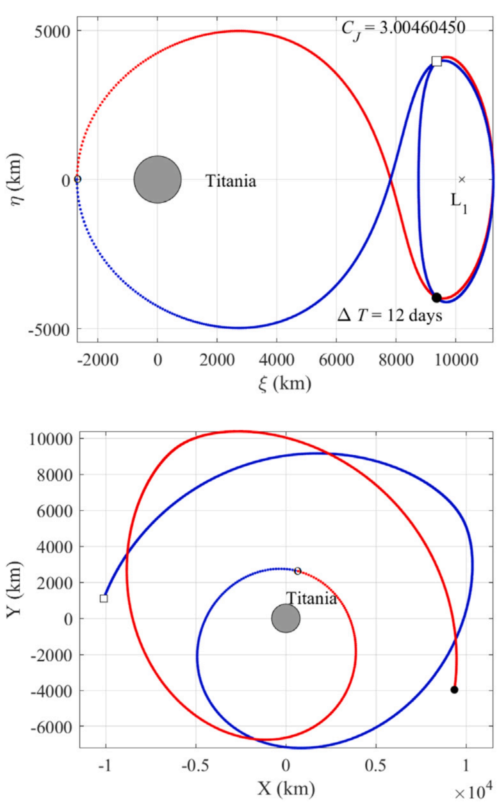

Fig. 12. Homoclinic connection in the Uranus–Titania system from/to a PLO around L_1 with $C_J = C_J^{**}$. Top: synodic moon-centered frame. Bottom: inertial moon-centered frame.

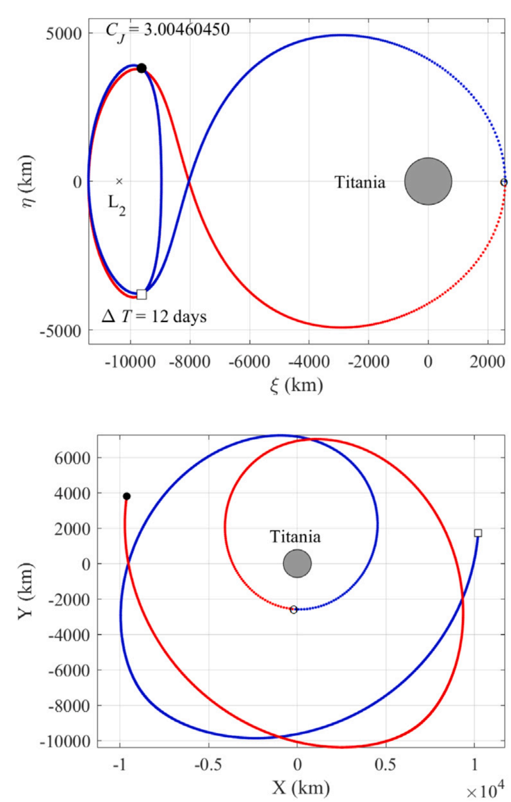

Fig. 14. Homoclinic connection in the Uranus–Titania system from/to a PLO around L_2 with $C_J = C_J^{**}$. Top: synodic moon-centered frame. Bottom: inertial moon-centered frame.

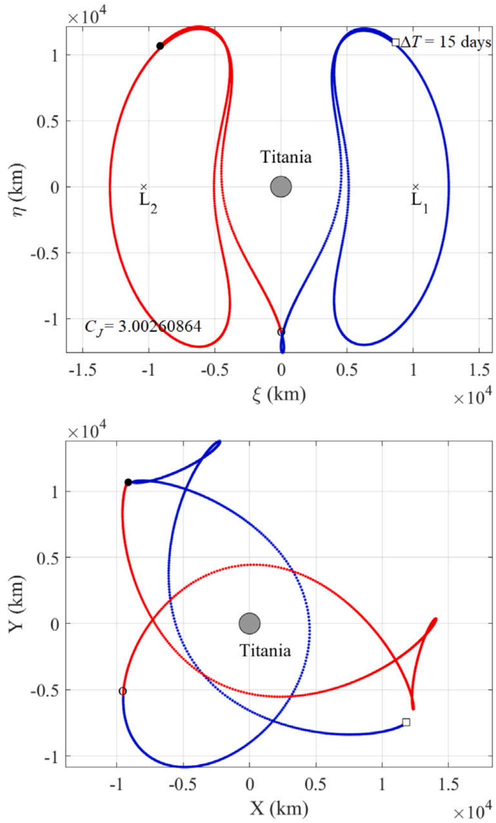

Fig. 15. Heteroclinic connection in the Uranus–Titania system from a PLO around L_2 to a PLO around L_1 with $C_J = C_J^*$. Top: synodic moon-centered frame. Bottom: inertial moon-centered frame.

Table 6
Minimum (h_{min}) and maximum (h_{max}) altitudes above the lunar surface, minimum (v_{min}) and maximum (v_{max}) speeds with respect to a moon-centered inertial frame, times of flight ΔT through the homoclinic connections of PLOs around L_2 with Jacobi constant C_J in the three systems considered.

CR3BP	C_J	h_{min} (km)	h_{max} (km)	v_{min} (m/s)	v_{max} (m/s)	ΔT (day)
Jupiter–Europa	C_J^*	404	18 573	32	1678	7
Jupiter–Europa	C_J^{**}	1222	13 357	133	1336	5
Uranus–Titania	C_J^*	1569	18 814	20	438	23
Uranus–Titania	C_J^{**}	1792	10 620	31	361	12
Uranus–Oberon	C_J^*	184	16 680	3	613	24
Uranus–Oberon	C_J^{**}	165	13 281	40	615	19

Table 7
Minimum (h_{min}) and maximum (h_{max}) altitudes above the lunar surface, minimum (v_{min}) and maximum (v_{max}) speeds with respect to a moon-centered inertial frame, times of flight ΔT of the spacecraft along the heteroclinic connections between PLOs at L_2 and L_1 with Jacobi constant C_J in the three systems considered.

CR3BP	C_J	h_{min} (km)	h_{max} (km)	v_{min} (m/s)	v_{max} (m/s)	ΔT (day)
Jupiter–Europa	C_J^*	4282	17 151	12	989	6
Jupiter–Europa	C_J^{**}	2241	14 266	8	1116	5
Uranus–Titania	C_J^*	3643	13 295	4	303	15
Uranus–Titania	C_J^{**}	1652	11 217	0.1	381	12
Uranus–Oberon	C_J^*	5288	16 423	1	233	23
Uranus–Oberon	C_J^{**}	3007	14 302	0.2	273	18

The closest approach to the moon is achieved with homoclinic connections of PLOs with the minimum Jacobi constant (C_J^*). As an example, the homoclinic connection of a PLO around L_2 with $C_J = C_J^*$ in the Jupiter–Europa system reaches a minimum altitude of 404 km above the surface of the moon. Also the lowest maximum speed is

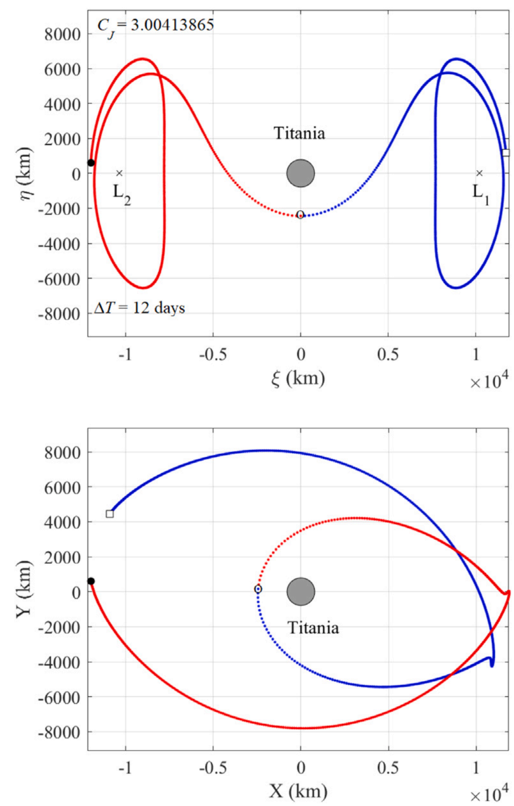

Fig. 16. Heteroclinic connection in the Uranus–Titania system from a PLO around L_2 to a PLO around L_1 with $C_J = C_J^{**}$. Top: synodic moon-centered frame. Bottom: inertial moon-centered frame.

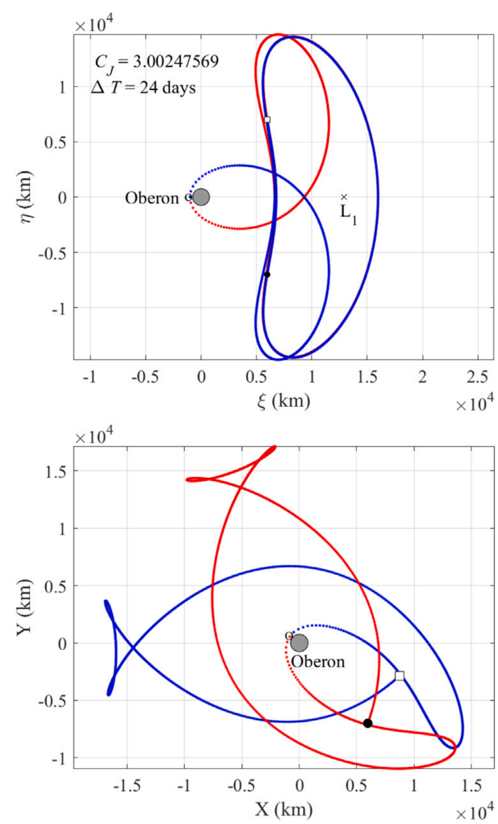

Fig. 17. Homoclinic connection in the Uranus–Oberon system from/to a PLO around L_1 with $C_J = C_J^*$. Top: synodic moon-centered frame. Bottom: inertial moon-centered frame.

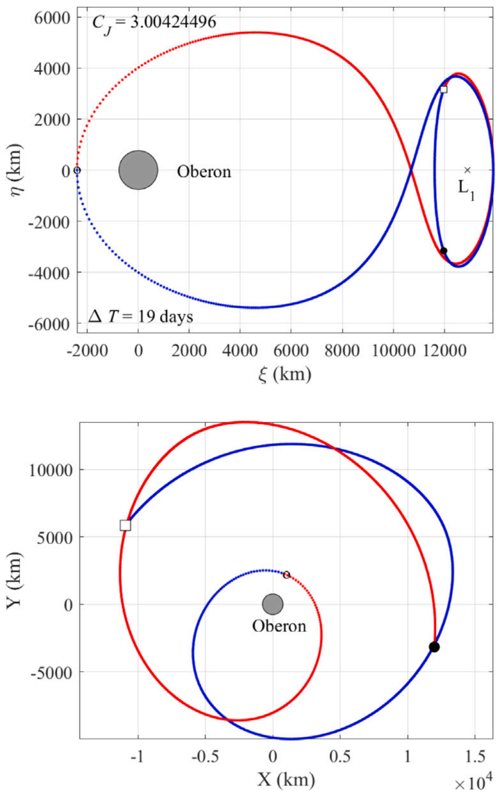

Fig. 18. Homoclinic connection in the Uranus–Oberon system from/to a PLO around L_1 with $C_J = C_J^{**}$. Top: synodic moon-centered frame. Bottom: inertial moon-centered frame.

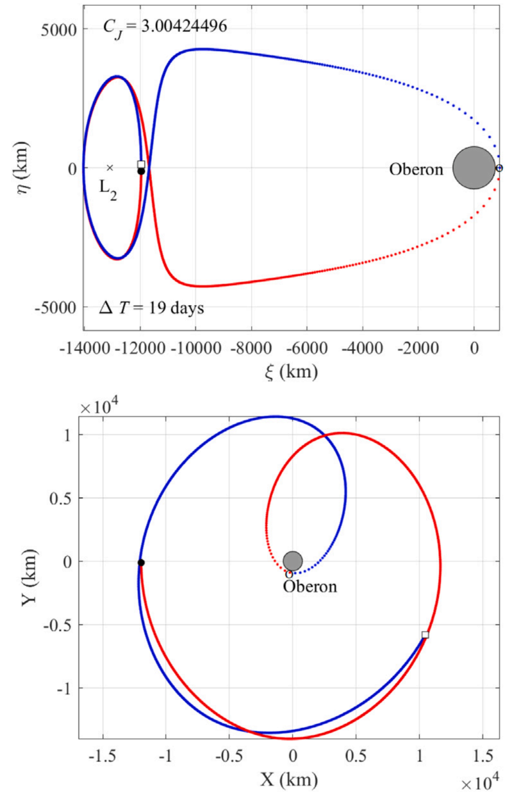

Fig. 20. Homoclinic connection in the Uranus–Oberon system from/to a PLO around L_2 with $C_J = C_J^{**}$. Top: synodic moon-centered frame. Bottom: inertial moon-centered frame.

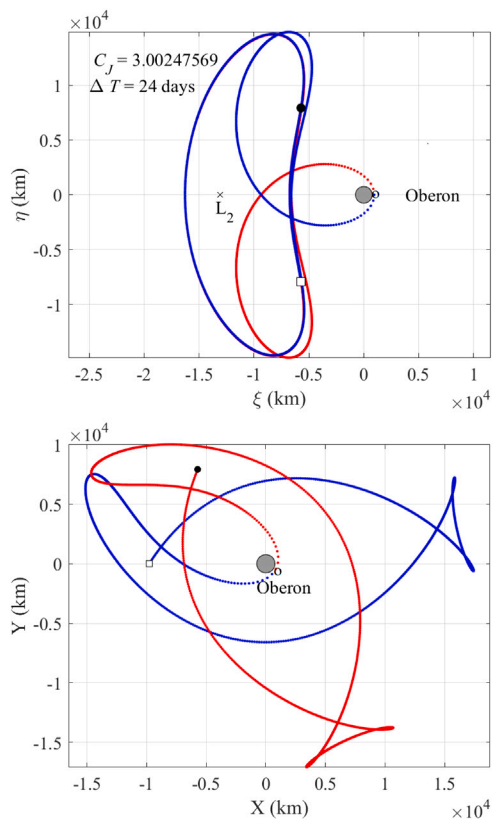

Fig. 19. Homoclinic connection in the Uranus–Oberon system from/to a PLO around L_2 with $C_J = C_J^{*}$. Top: synodic moon-centered frame. Bottom: inertial moon-centered frame.

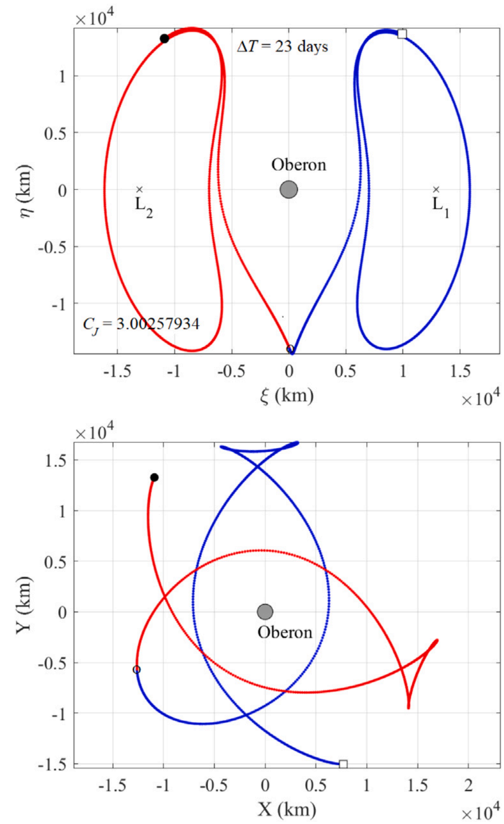

Fig. 21. Heteroclinic connection in the Uranus–Oberon system from a PLO around L_2 to a PLO around L_1 with $C_J = C_J^{*}$. Top: synodic moon-centered frame. Bottom: inertial moon-centered frame.

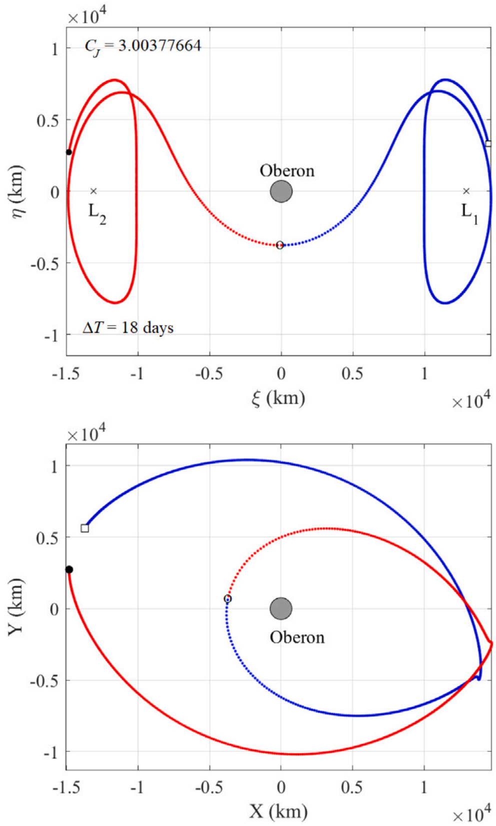

Fig. 22. Heteroclinic connection in the Uranus–Oberon system from a PLO around L_2 to a PLO around L_1 with $C_J = C_J^{**}$. Top: synodic moon-centered frame. Bottom: inertial moon-centered frame.

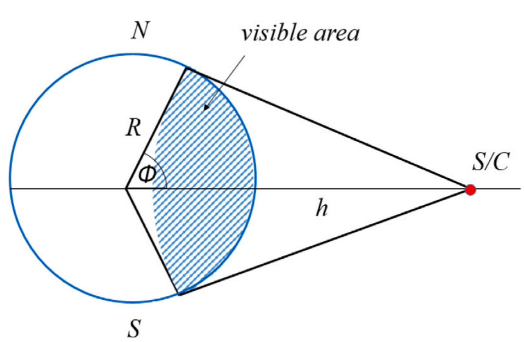

Fig. 23. Maximum visible latitude ϕ from an altitude h above the equator of a spherical body of radius R.

Table 8
Ranges of maximum visible latitude through the homoclinic and heteroclinic transfers shown in Figs. 6–22.

CR3BP	C_J	Homoclinic L_1	Homoclinic L_2	Heteroclinic
Jupiter–Europa	C_J^*	39°–86°	37°–86°	76°–85°
Jupiter–Europa	C_J^{**}	60°–84°	56°–84°	65°–84°
Uranus–Titania	C_J^*	68°–88°	71°–88°	81°–87°
Uranus–Titania	C_J^{**}	73°–86°	72°–86°	71°–86°
Uranus–Oberon	C_J^*	41°–87°	20°–87°	83°–87°
Uranus–Oberon	C_J^{**}	72°–87°	34°–87°	78°–87°

in general associated with the heteroclinic connections at the minimum Jacobi constant level. The time of flight and, therefore, the time that can be devoted to the observations is not longer on heteroclinic transfers. The pericenter altitudes and the times of flight along the heteroclinic connections computed for the Uranus–Oberon system are much higher than those obtained in the equivalent connections in the Uranus–Titania system, which might be a consequence of the different orbital periods of the two moons.

The axial tilt of all the moons considered is approximately zero. In other words, the moon's equator is contained in the orbital plane of the spacecraft. So, for planar trajectories, the instantaneous coverage from an altitude h above the lunar surface can be determined by computing the maximum visible latitude ϕ (see Fig. 23):

$$\phi = \cos^{-1}\left(\frac{R}{R+h}\right), \tag{4}$$

where R is the radius of the moon, specified in Table 1. The maximum visible latitude ϕ for the homoclinic and heteroclinic transfers displayed in Figs. 6–22 are reported in Table 8. The ranges of ϕ account for the varying distance from the surface of the moon along the transfer. This fact can be appreciated in Figs. 24–29 that illustrate the instantaneous surface coverage as a function of time t with $0 \le t \le \Delta T$ along a representative sample of transfers. Even though the altitude above the surface is quite high (more than 10000 km) for most of the time, a wide equatorial band (indicated by a box in the figures) is visible during the close approaches (which reach as low as 300 km in the case of Oberon) and these uninterrupted observation windows last several hours.

4. Conclusions

This investigation proposes the use of three-body dynamics to overfly and observe the surface of three moons, i.e., Europa, Titania, and Oberon. The motivation resides in the strong scientific interest towards these objects, which is boosting a number of plans for their robotic exploration. This work analyzes a possible orbital infrastructure to support these scientific plans and provides performance parameters to lay out a solid observing program.

The focus is on the dynamics in the vicinity of the collinear libration points L_1 and L_2 in the circular restricted three-body problem with a moon and its planet as primaries. It is known that the stable and unstable hyperbolic invariant manifolds of libration point orbits can be linked in the phase space to form homoclinic and heteroclinic trajectories. This category of orbits have been employed in space mission design to transfer a probe to its final destination. Here, homoclinics and heteroclinics are proposed because their patterns of motion drive the third body, i.e., the spacecraft, to loop around the moon while flying between libration point orbits. The departure and destination orbits themselves play an important role in this mission scenario as they can serve as science orbits, parking orbits between transfers and gates towards nearby moons in the same planetary system. The primaries are spherical homogeneous bodies and the motion develops in the xy-plane. A recent investigation on halo orbits around L_1 and L_2 of the Saturn–Enceladus system [33] provides insight into the performance of 3D heteroclinic and homoclinic connections for the observation of the lunar poles and completes the analysis presented here. The effect of the second zonal harmonic of the primaries on these 3D solutions is also being considered: equivalent transfer orbits can be reconstructed in the perturbed model and their observing properties do not differ substantially from those of the unperturbed model, proving that the latter can be straightforwardly used in preliminary analyses.

The planar Lyapunov orbits employed in this work to design heteroclinic and homoclinic connections span an energy range wide enough to provide insight into the patterns of motion of the spacecraft and quantify the observational performance of the proposed science orbits. The analysis shows that the surface of the moons can be observed from very low (300 km in the case of Oberon) to moderate altitudes (2500–4000 km) and with low relative speeds (always below 1 km/s and reaching below 1 m/s). The mission scenarios that arise are appealing as they offer long and uninterrupted views of large fractions of the lunar surface, symmetrical with respect to the equator.

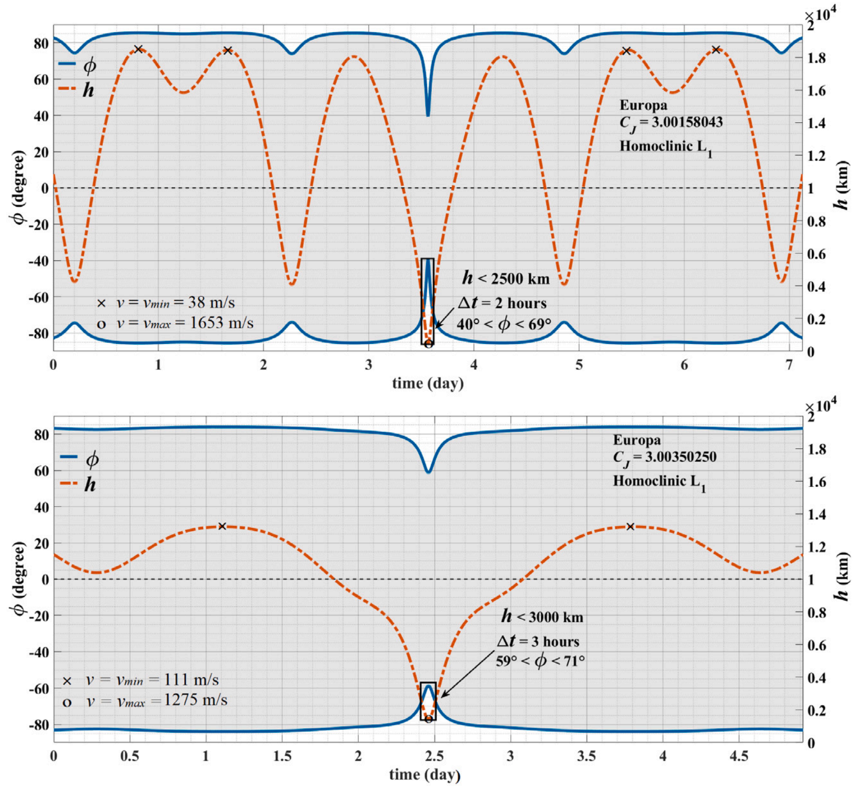

Fig. 24. Altitude above the lunar surface and maximum visible latitude ϕ as functions of time through L_1 homoclinic connections corresponding to C_J^* (top) and C_J^{**} (bottom) in the Jupiter–Europa system.

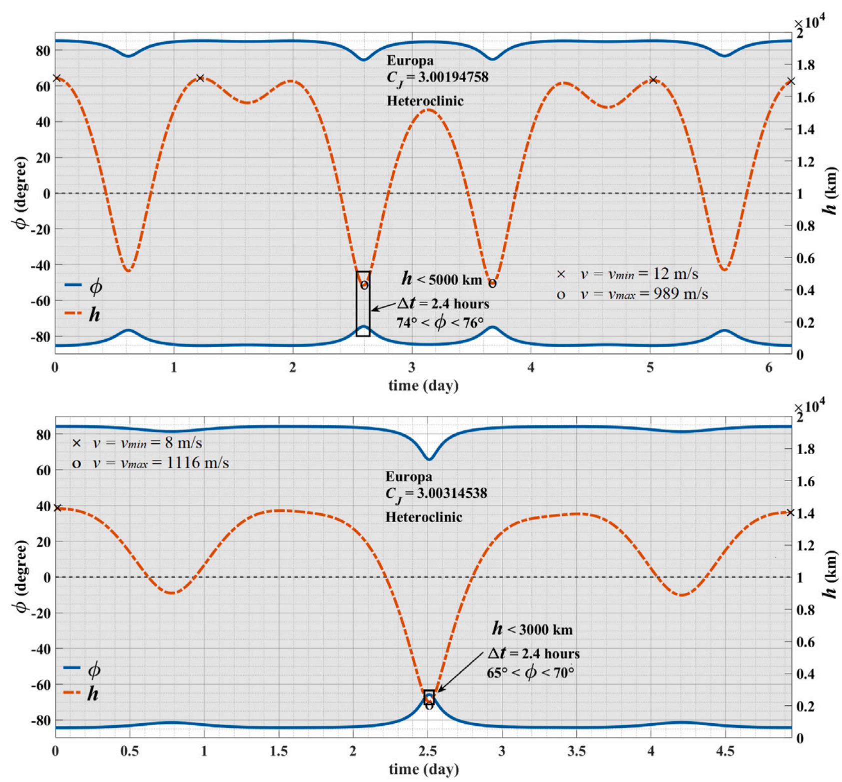

Fig. 25. Altitude above the lunar surface and maximum visible latitude ϕ (degree) as functions of time through the heteroclinic connections corresponding to C_J^* (top) and C_J^{**} (bottom) in the Jupiter–Europa system.

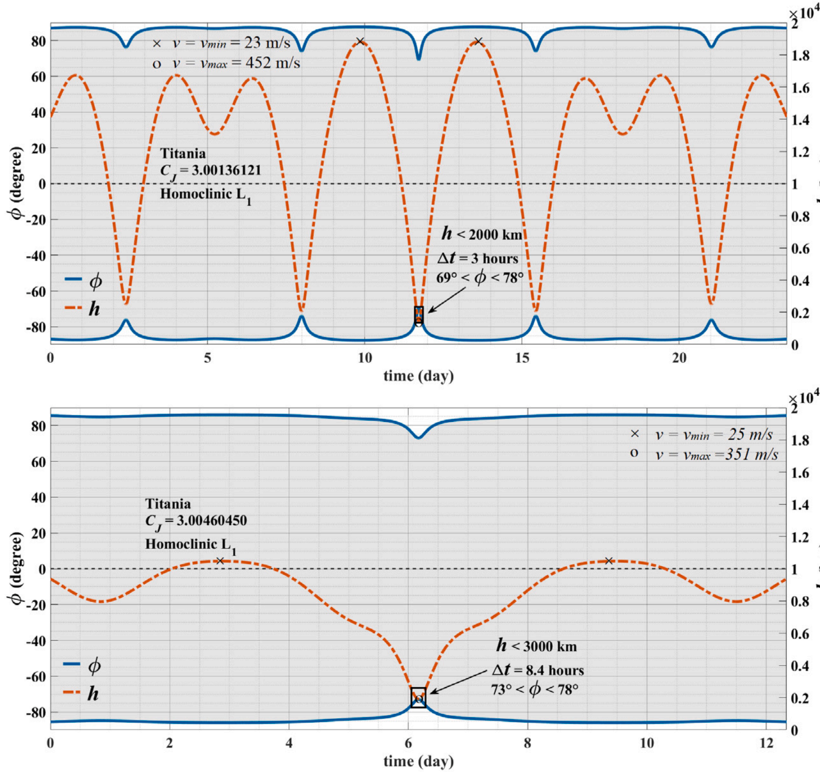

Fig. 26. Altitude above the lunar surface and maximum visible latitude ϕ as functions of time through L_1 homoclinic connections corresponding to C_J^* (top) and C_J^{**} (bottom) in the Uranus–Titania system.

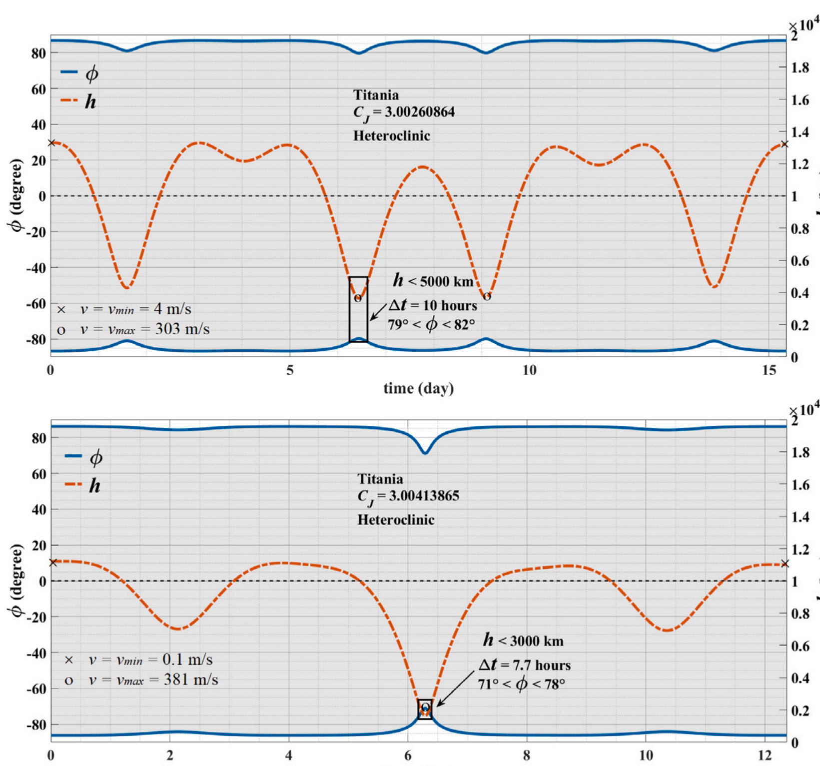

Fig. 27. Altitude above the lunar surface and maximum visible latitude ϕ as functions of time through heteroclinic connections corresponding to C_J^* (top) and C_J^{**} (bottom) in the Uranus–Titania system.

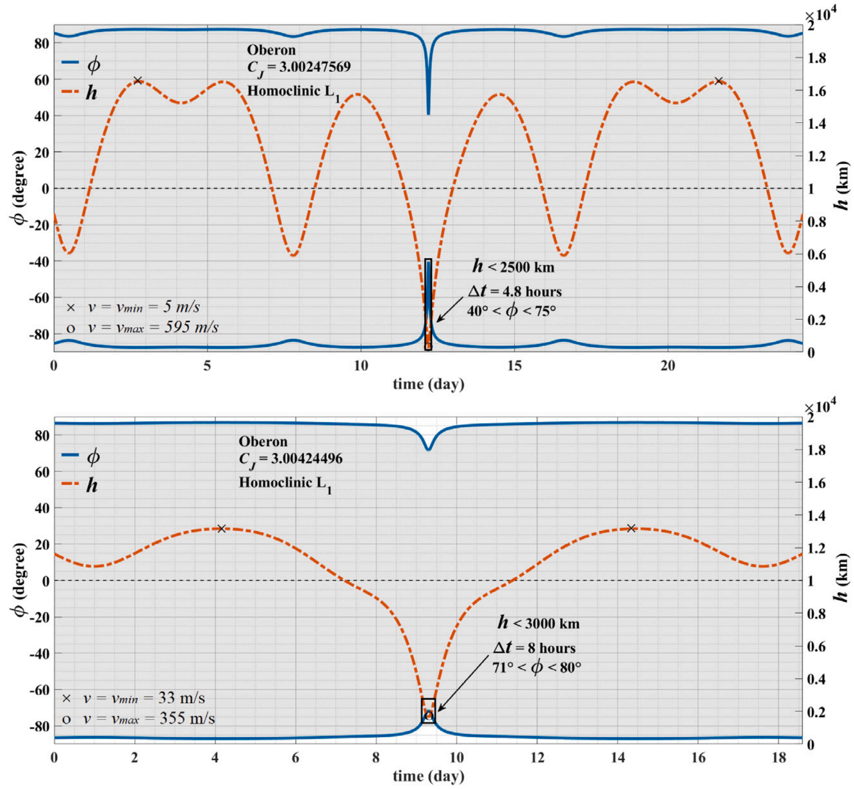

Fig. 28. Altitude above the lunar surface and maximum visible latitude ϕ as functions of time through L_1 homoclinic connections corresponding to C_J^* (top) and C_J^{**} (bottom) in the Uranus–Oberon system.

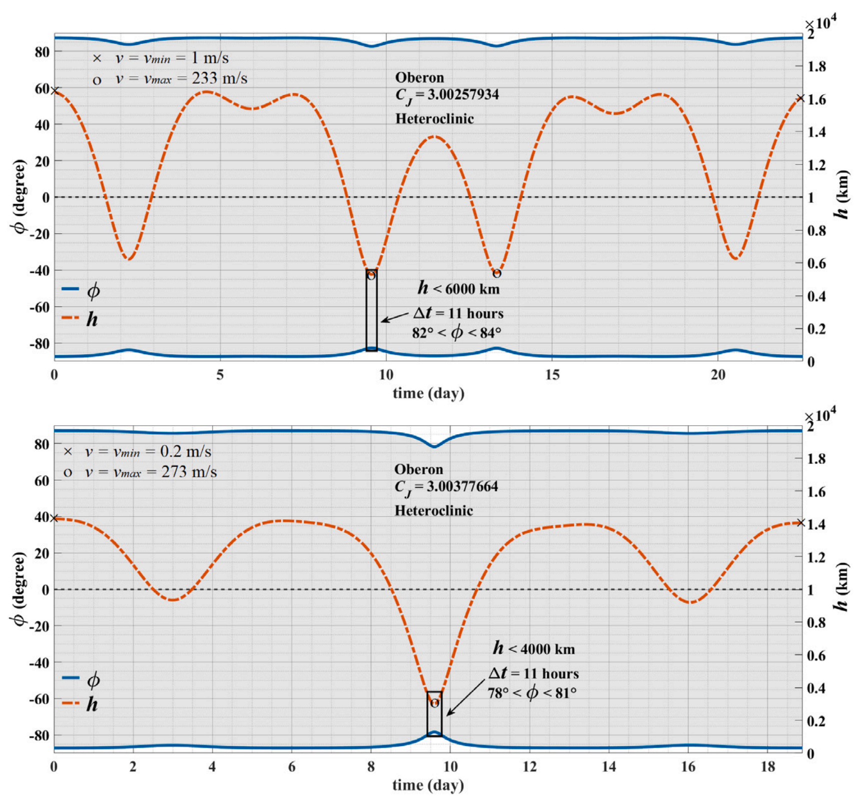

Fig. 29. Altitude above the lunar surface and maximum visible latitude ϕ as functions of time through heteroclinic connections corresponding to C_J^* (top) and C_J^{**} (bottom) in the Uranus–Oberon system.

In conclusion, low-energy trajectories are a viable option for planetary exploration missions beyond the Earth–Moon system (see [38–41]). This contribution focuses on the observational features of heteroclinic and homoclinic connections associated with L_1/L_2 planar Lyapunov orbits, but the proposed methodology can be applied to other types of low-energy orbits. In particular, the benefits of planar orbits can be further assessed by addressing the distant prograde orbits. This type of solutions were exploited by WIND in the Sun–Earth system [42] and analyzed in detail along with their relationship with the planar Lyapunov orbits in [39,43,44].

Declaration of competing interest

The authors declare that they have no known competing financial interests or personal relationships that could have appeared to influence the work reported in this paper.

Acknowledgments

The authors thank the reviewers for their constructive comments, which helped to improve the manuscript. This work has been supported by Khalifa University of Science and Technology's internal grants FSU-2018-07 and CIRA-2018-085.

References

[1] D.J. Scheeres, M.D. Guman, B.F. Villac, Stability analysis of planetary satellite orbiters: application to the Europa orbiter, J. Guid. Control Dyn. 24 (2001) 778–787, http://dx.doi.org/10.2514/2.4778.
[2] M. Lara, J.F. San-Juan, Dynamic behavior of an orbiter around Europa, J. Guid. Control Dyn. 28 (2005) 291–297, http://dx.doi.org/10.2514/1.5686.
[3] M.E. Paskowitz, D.J. Scheeres, Robust capture and transfer trajectories for planetary satellite orbiters, J. Guid. Control Dyn. 29 (2006) 342–353, http://dx.doi.org/10.2514/1.13761.
[4] M.E. Paskowitz, D.J. Scheeres, Design of science orbits about planetary satellites: application to Europa, J. Guid. Control Dyn. 29 (2006) 1147–1158, http://dx.doi.org/10.2514/1.19464.
[5] R.P. Russell, Global search for planar and three-dimensional periodic orbits near Europa, J. Astron. Sci. 54 (2006) 199–226, http://dx.doi.org/10.1007/BF03256483.
[6] R.P. Russell, M. Lara, On the design of an enceladus science orbit, Acta Astronaut. 65 (2009) 27–39, http://dx.doi.org/10.1016/j.actaastro.2009.01.021.
[7] V. Szebehely, Theory of Orbits, Academic Press, New York, 1967.
[8] G. Gómez, W.S. Koon, M.W. Lo, J.E. Marsden, J.J. Masdemont, S.D. Ross, Connecting orbits and invariant manifolds in the spatial restricted three-body problem, Nonlinearity 17 (5) (2004) 1571–1606, http://dx.doi.org/10.1088/0951-7715/17/5/002.
[9] E. Canalias, J.J. Masdemont, Homoclinic and heteroclinic transfer trajectories between planar Lyapunov orbits in the Sun–Earth and Earth–Moon systems, Discrete Contin. Dyn. Syst. 14 (2) (2006) 262–279, http://dx.doi.org/10.3934/dcds.2006.14.261.
[10] E. Barrabés, J.M. Mondelo, M. Ollé, Numerical continuation of families of homoclinic connections of periodic orbits in the RTBP, Nonlinearity 22 (12) (2009) 2901–2918, http://dx.doi.org/10.1088/0951-7715/22/12/006.
[11] M.B. Quadrelli, L.J. Wood, J.E. Riedel, et al., Guidance, navigation, and control technology assessment for future planetary science missions, J. Guid. Control Dyn. 38 (7) (2015) 1165–1186, http://dx.doi.org/10.2514/1.G000525.
[12] K.C. Howell, B.T. Barden, R.S. Wilson, M. Lo, Trajectory design using a dynamical systems approach with application to GENESIS, in: AAS/AIAA Astrodynamics Specialist Conference, Sun Valley, Idaho, 1997, paper AAS 97-709.
[13] M. Woodard, D. Folta, D. Woodfork, ARTEMIS: the first mission to the lunar libration orbits, in: 21st International Symposium on Space Flight Dynamics, Toulouse, France, 2009.
[14] W.S. Koon, M.W. Lo, J.E. Marsden, S.D. Ross, Constructing a low energy transfer between Jovian moons, Contemp. Math. Am. Soc. 292 (2002) 129–145.
[15] D.C. Davis, S.M. Phillips, B.P. McCarthy, Trajectory design for Saturnian ocean worlds orbiters using multidimensional Poincaré maps, Acta Astronaut. 143 (2018) 16–28, http://dx.doi.org/10.1016/j.actaastro.2017.11.004.
[16] E. Fantino, E.M. Alessi, J. Peláez, Connecting low-energy orbits in the Saturn system, in: 18th Australian Aerospace Congress, in: Melbourne, Australia, 2019.
[17] P. Pergola, K. Geurts, C. Casaregola, M. Andrenucci, Power constrained Uranus transfer and moons tour by three body invariant manifolds and electric propulsion, in: 18th AAS/AIAA Space Flight Mechanics Meeting, Galveston, Texas, 2008, paper AAS 08-196.
[18] W.S. Koon, M.W. Lo, J.E. Marsden, S.D. Ross, Dynamical Systems, The Three-Body Problem and Space Mission Design, Marsden Books, 2011.
[19] E.M. Alessi, P. Pergola, Two options for the Callisto's exploration, Acta Astronaut. 72 (2012) 185–197, http://dx.doi.org/10.1016/j.actaastro.2011.09.003.
[20] National Research Council, Vision and Voyages for Planetary Science in the Decade 2013-2022, Tech. Rep., The National Academies Press, Washington, D.C., 2011.
[21] W.M. Grundy, J.R. Spencer, R.E. Johnson, E.F. Young, M.W. Buie, Distributions of H2O and CO2 ices on Ariel, Umbriel, Titania, and Oberon from IRTF/SpeX observations, Icarus 184 (2006) 534–555, http://dx.doi.org/10.1016/j.icarus.2006.04.016.
[22] C.C. Porco, P. Helfenstein, P.C. Thomas, et al., Cassini observes the active south pole of Enceladus, Science 311 (2006) 1393–1401, http://dx.doi.org/10.1126/science.1123013.
[23] J.R. Spencer, J.C. Pearl, M. Segura, et al., Cassini encounters enceladus: background and the discovery of a south polar hot spot, Science 311 (2006) 1401–1405, http://dx.doi.org/10.1126/science.1121661.
[24] N. Khawaja, F. Postberg, J. Hillier, et al., Low-mass nitrogen-, oxygen-bearing, and aromatic compounds in Enceladean ice grains, Mon. Not. R. Astron. Soc. 489 (2019) 5231–5243, http://dx.doi.org/10.1093/mnras/stz2280.
[25] J.C. Cook, R. Gutro, D. Brown, et al., Hubble sees evidence of water vapor at Jupiter moon, 2013, https://www.jpl.nasa.gov/news/news.php?release=2013-363, (Accessed 27 September 2019).
[26] C.S. Arridge, C.B. Agnor, N. André, et al., Uranus pathfinder: exploring the origin and evolution of Ice Giant planets, Exp. Astron. 33 (2012) 753–791, http://dx.doi.org/10.1007/s10686-011-9251-4.
[27] The JUICE Science Working Team, JUICE Jupiter Icy Moons Explorer, Exploring The Emergence of Habitable Worlds Around Gas Giants, Tech. Rep., ESA, 2014, ESA/SRE(2014) 1.
[28] R. Pappalardo, et al., The Europa Clipper – OPAG Update, Tech. Rep., JPL/APL, 2013, JPL/APL Report.
[29] C.S. Arridge, N. Achilleos, J. Agarwal, et al., The science case for an orbital mission to Uranus: exploring the origins and evolution of ice giant planets, Planet. Space Sci. 104 (2014) 122–140, http://dx.doi.org/10.1016/j.pss.2014.08.009.
[30] D. Turrini, R. Politi, R. Peron, et al., The ODINUS mission concept - the scientific case for a mission to the ice giant planets with twin spacecraft to unveil the history of our solar system, 2013, http://odinus.iaps.inaf.it/wp.php, (Accessed 1 February 2020).
[31] C.M. Elder, A.M. Bramson, L.W. Blum, et al., New frontiers-class missions to the ice giants, in: Planetary Science Vision 2050 Workshop, Washington, D.C., 2017.
[32] Jet Propulsion Laboratory, Planetary satellite mean orbital parameters, 2019, https://ssd.jpl.nasa.gov/?sat_elem, (Accessed 27 September 2019).
[33] E. Fantino, F. Salazar, E.M. Alessi, Design and performance of low-energy orbits for the exploration of enceladus, Commun. Nonlinear Sci. Numer. Simul. 90 (2020) 105393, http://dx.doi.org/10.1016/j.cnsns.2020.105393.
[34] E. Fantino, R. Castelli, Efficient design of direct low-energy transfers in multi-moon systems, Celestial Mech. Dynam. Astronom. 127 (2017) 429–450, http://dx.doi.org/10.1007/s10569-016-9733-9.
[35] A. Viale, Low-energy Tour of the Galilean Moons (Master's thesis), Università degli Studi di Padova, Italy, 2016.
[36] R.P. Russell, N.F. Strange, Planetary moon cycler trajectories, J. Guid. Control Dyn. 32 (2009) 143–157, http://dx.doi.org/10.2514/1.36610.
[37] T.S. Parker, L. Chua, Practical Numerical Algorithms for Chaotic Systems, Springer-Verlag, New York, 1989.
[38] M. Woodard, D. Folta, D. Woodfork, ARTEMIS: The first mission to the lunar libration points, in: 21st International Symposium on Space Flight Dynamics, Toulouse, France, 2009.
[39] D.C. Folta, N. Bosanac, D. Guzzetti, K.C. Howell, An earth-moon system trajectory design reference catalog, Acta Astronaut. 110 (2015) 341–353, http://dx.doi.org/10.1016/j.actaastro.2014.07.037.
[40] D. Folta, M. Woodard, Design and implementation of the ARTEMIS lunar transfer using multi-body dynamics, in: AAS/AIAA Astrodynamics Specialist Conference, Girdwood, Alaska, 2011, paper AAS 11-511.
[41] S.B. Broschart, T.H. Sweetser, V. Angelopoulos, et al., ARTEMIS lunar orbit insertion and science orbit design through 2013, in: AAS/AIAA Strodynamics Specialist Conference, Girdwood, Alaska, 2011, paper AAS 11-509.
[42] C.E. Roberts, Long term missions at the Sun-Earth Libration Point L1: ACE, SOHO and WIND, in: AAS/AIAA Strodynamics Specialist Conference, Girdwood, Alaska, 2011, paper AAS 11-485.
[43] J.S. Parker, K.E. Davis, G.H. Born, Chaining periodic three-body orbits in the earth-moon system, Acta Astronaut. 67 (2010) 623–638, http://dx.doi.org/10.1016/j.actaastro.2010.04.003.
[44] A. Haapala, M. Vaquero, T. Pavlak, et al., Trajectory selection strategy for tours in the Earth-Moon system, in: AAS/AIAA Astrodynamics Specialist Conference, Hilton Head, South Carolina, 2013, paper AAS 13-782.